Korean J. Chem. Eng., 36(6), 851-859 (2019)
DOI: 10.1007/s11814-019-0275-1

pISSN: 0256-1115
eISSN: 1975-7220

Composition modulation of $Cu/Cu_2O/CuO$ nanoparticles supported on carbon for *p*-nitrophenol reduction

Jia Li, Wei Liu, Yongxin Ding, Likui Liu, Fang Li, and Qiming Li†

College of Chemistry, Chemical Engineering and Environmental Engineering, Liaoning Shihua University, Fushun Liaoning 113001, P. R. China

(*Received 21 January 2019 • accepted 9 April 2019*)

Abstract−Porous carbon supported $Cu/Cu_2O/CuO$ ternary catalysts were fabricated by pyrolysis, in which composition modulation of $Cu/Cu_2O/CuO$ was successfully realized by adjusting annealing atmosphere. The correlation between annealing atmosphere and composition of $Cu/Cu_2O/CuO$ ternary nanoparticles was deeply investigated. XRD and SEM measurement shows that the composition proportion of $Cu/Cu_2O/CuO$ can be effectively controlled by adjusting the annealing atmosphere. HR-TEM and EDS analysis showed that $Cu/Cu_2O/CuO$ ternary nanoparticles are highly dispersed into the carbon matrix and harvest more hetero-junction active sites. The effect of $Cu/Cu_2O/CuO$ composition on their catalytic activity was investigated in catalytic reduction from *p*-nitrophenol to *p*-aminophenol. The experimental result indicated that the catalytic activity of $Cu/Cu_2O/CuO$ ternary catalysts exhibits higher catalytic activity than Cu_2O/CuO or CuO particles. This work provides a new strategy for synthesizing and modulating porous carbon-supported $Cu/Cu_2O/CuO$ ternary nanoparticles.

Keywords: Ternary Catalysts, Annealing, Composition Modulation, Phase Structure, Catalytic Activity

INTRODUCTION

The green treatment of wastewater containing different organic contaminants such as benzene [1], phenol [2], aromatics [3] or nitrophenol [4] has attracted much attention. And the catalytic degradation of these organic contaminants in wastewater is an environment-friendly solution. For instance, *p*-nitrophenol is considered as one of the most refractory pollutants present in industrial effluents, but *p*-aminophenol is an important intermediate in the preparation of drugs such as paracetamol, acetanilide, phenacetin [5-7]. Hence, it is significant to transform *p*-nitrophenol into *p*-aminophenol by a green chemical process.

It is well known that precious metals have excellent catalytic activity and stability in catalytic transformation of *p*-nitrophenol [8-10], but the high cost of noble metals limits their widespread application. Alternatively, some transition metal nanoparticles display a better applicable prospect due to lower cost, versatile functions and moderate activity [11-14]. Amongst these transition metallic nanoparticles, the valence state of copper can thermodynamically change amongst Cu, Cu_2O and CuO, and thus it provides a possibility to assemble $Cu/Cu_2O/CuO$ ternary nanoparticles, which endows versatile catalytic functions [15]. Hence, it is reported that copper-based nanoparticles possess higher catalytic activity in the catalytic reduction from *p*-nitrophenol into *p*-aminophenol [16,17]. However, it is difficult to rationally control the composition of $Cu/Cu_2O/CuO$ ternary nanoparticles by traditional method [18]. Although the mechanical mixing of Cu,Cu_2O and CuO particles can adequately modulate the ternary composition, the synergistic effect of $Cu/Cu_2O/CuO$ ternary nanoparticles will be seriously weakened. This is because the interface-exposed hetero-junctions of $Cu/Cu_2O/CuO$ nanocomposites play a more important role in catalytic reaction. In addition, the surfaces of Cu or Cu_2O nanoparticles are readily oxidized to form CuO passivation layer, resulting in the isolation of Cu phase, Cu_2O phase and CuO phase [19,20]. To inhibit surface oxidation and improve dispersity of $Cu/Cu_2O/CuO$ nanocomposites, some solid supports such as zeolites, MOFs, activated carbons or solid polymers, can be used to support $Cu/Cu_2O/CuO$ composite nanoparticles [21-23]. Among them, porous carbon can provide higher specific surface area and good electron conductivity for Cu-based nanoparticles. Therefore, it is significant to modulate the composition of ternary nanoparticles and further fabricate porous carbon supported $Cu/Cu_2O/CuO$ nanoparticles by single step [24,25].

Metal-organic frameworks (MOFs) as novel porous materials are attracting much attention due to ultra-high surface area, fascinating adsorption affinity, and facilely tailorable functionalities [26-28]. Based on MOFs, versatile carbon materials are developed by pyrolysis in inert atmosphere, where organic ligands are transformed into porous skeleton graphical carbon, and metals ions are transformed into the corresponding metals or metal oxide [29]. Bak et al. developed a facile method to transform MOFs into metal/metal oxide@carbon (M/MO@C) composites with well-defined shapes [30]. Hu et al. fabricated Co_3O_4 porous nanocages by the thermal decomposition of Prussian blue analogue (PBA) $Co_3[Co(CN)_6]_2$ truncated nanocubes at 400 °C [1]. Zhang et al. synthesized Cu/CuOx/C nanocomposites based on Cu-HKUST-1 precursors [31]. However, traditional carbon-encapsulated nanoparticles were prepared under single atmosphere, and the composition of composite nanoparticles cannot be modulated. To our knowledge, a rational

†To whom correspondence should be addressed.
E-mail: lqm_dicp@163.com

Table 1. Synthesis conditions of different Cu-based metal-organic frameworks

Sample	Synthesis solution	Solvent	Synthesis temperature (°C)	Synthesis time (h)
Sample A	$Cu(NO_3)_2$/BTC	Ethanol/H_2O	120	72
Sample B	$Cu(NO_3)_2$/BTC	Ethanol/H_2O	120	4
Sample C	$Cu(NO_3)_2$/BTC/PVP	Ethanol/H_2O	120	4
Sample D	$Cu(NO_3)_2$/BTC/PVP	Ethanol/H_2O	100	4

composition modulation of Cu/Cu_2O/CuO ternary nanoparticles by pyrolyzing MOFs is rarely reported.

In this article, we report a facile method to modulate the composition of Cu/Cu_2O/CuO ternary nanoparticles supported by porous graphitic carbon. The rational composition optimization of Cu/Cu_2O/CuO ternary nanoparticles was realized by tuning annealing atmosphere. The effect of annealing atmosphere and sintering temperature on composition and microstructure of Cu/Cu_2O/CuO ternary nanoparticles was investigated in detail. Meanwhile, the catalytic activity of porous carbon supported Cu/Cu_2O/CuO ternary nanoparticles was also checked by the catalytic reduction of *p*-nitrophenol to *p*-aminophenol.

MATERIALS AND METHODS

1. Optimization of Cu-BTC

Cu-BTC was synthesized by a modified solvothermal method. Typically, 0.8 g $Cu(NO)_3{\cdot}5H_2O$ and 0.1 g PVP(polyvinylpyrrolidone) are dissolved into 30 ml of methanol. After stirring for 30 min, a blue transparent methanol solution can be obtained. Another methanol solution was obtained by mixing 0.4 g BTC (1,3,5-benzenetricarboxylate) and 30 ml methanol. Then, two mixed solutions were mixed together and stirred for 10 min to obtain a blue solution. The final mixed solution was put into a 100 ml autoclave and heated in a heating oven for 4 hrs at 393 K. The resulting blue precipitates were collected by filtration, washed with ethanol and methanol subsequently for three times, and finally vacuum-dried at 90 °C for 12 hrs. Other samples used in this article were synthesized with a similar procedure, and their respective conditions are listed in Table 1.

2. Preparation of Carbon-supported Cu/Cu_2O/CuO Ternary Nanoparticles

The obtained Cu-BTC nanoparticles were annealed at different temperature and annealing atmosphere by the following procedures: First, the as-prepared Cu-BTC samples were transferred in an alumina crucible. The crucible containing Cu-BTC was then put into a tube furnace. Before heating, the Cu-BTC samples should be purged for 30 min with the corresponding annealing gas stream to discharge all the oxygen. The Cu-BTC samples were annealed at different atmospheres for 180min, respectively, with a heating and cooling rate of 2 °C·min^{-1}. Note that the Cu-BTC samples should be protected during the whole heating and cooling procedure. The corresponding annealing atmosphere composition of all the samples is shown in Table 2.

3. Characterization

The surface morphology of all the samples was observed by a scanning electron microscope (SU8010) operating at 80 kV. The powder X-ray diffraction (XRD) patterns of the samples were collected on a Geman D8 Advance X-ray diffractometer equipped with Cu Kα radiation over the 2θ range of 10-70° (λ=0.1540). Energy dispersive X-ray spectroscopy (SEM-EDS) was also taken on the SU8010 scanning electron microscope. The surface morphology and particle microstructure of Cu/Cu_2O/CuO ternary nanoparticles were examined by high-resolution transmission electron microscope (HR-TEM, JEM-2100F). The UV-visible absorption spectra were recorded on UV-*vis* spectrophotometer (L5S, Shanghai Inesa Analytical Instrument Co. Ltd., China).

Table 2. EDS elemental analysis for the samples

Sintering atmosphere	Sintering temperature (°C)	Composition (At%)		
		C	Cu	O
Air	500 °C	8.12	75.82	16.06
N_2	500 °C	73.22	9.08	16.98

4. Catalytic Test

A *p*-nitrophenol reduction experiment was performed in our homemade apparatus at room temperature. The reduction reaction were performed by mixing 3.0 ml aqueous *p*-nitrophenol solution (0.0200 g·L^{-1}) with 0.1 m1 freshly prepared aqueous $NaBH_4$ solution (10.0 g·L^{-1}) in a 3 ml quartz cuvette. Subsequently, the color of aqueous *p*-nitrophenol solution turned yellow rapidly. Then, 1.0 mg of the catalyst was put into the above reaction mixture to start the reaction. Immediately, the subsequent reaction rate was *in-situ* monitored using L5S UV-*vis* spectroscopy over a scanning range of 200-500 nm and the successive spectral absorption changes could be collected with an interval of 30 s. The rate constant of the reaction was measured by the extinction of the solution at 400 nm as a function of time.

RESULTS AND DISCUSSION

1. Analysis of Cu-BTC Samples

In our experiment, Cu-BTC (HKUST-1) samples were prepared at different synthesis conditions as shown in Table 1. Fig. 1 shows SEM images of Cu-BTC samples. As shown in Fig. 1(a), sample A exhibits irregular polyhedral morphology and the particle size of most Cu-BTC particles is over 20 μm. Compared with sample A, the solvothermal time of sample B was shortened to 4 hrs, but sample B still displayed irregular polyhedral shape. While PVP was added into the synthesis solution, sample C was obtained under 120 °C for 4 hrs. It can be found that sample C exhibits regular polyhedral morphologies and its average particle size obviously decreases to about 600-800 nm. It can be concluded that the addition of PVP in precursor solution can harvest more uniform and well-defined

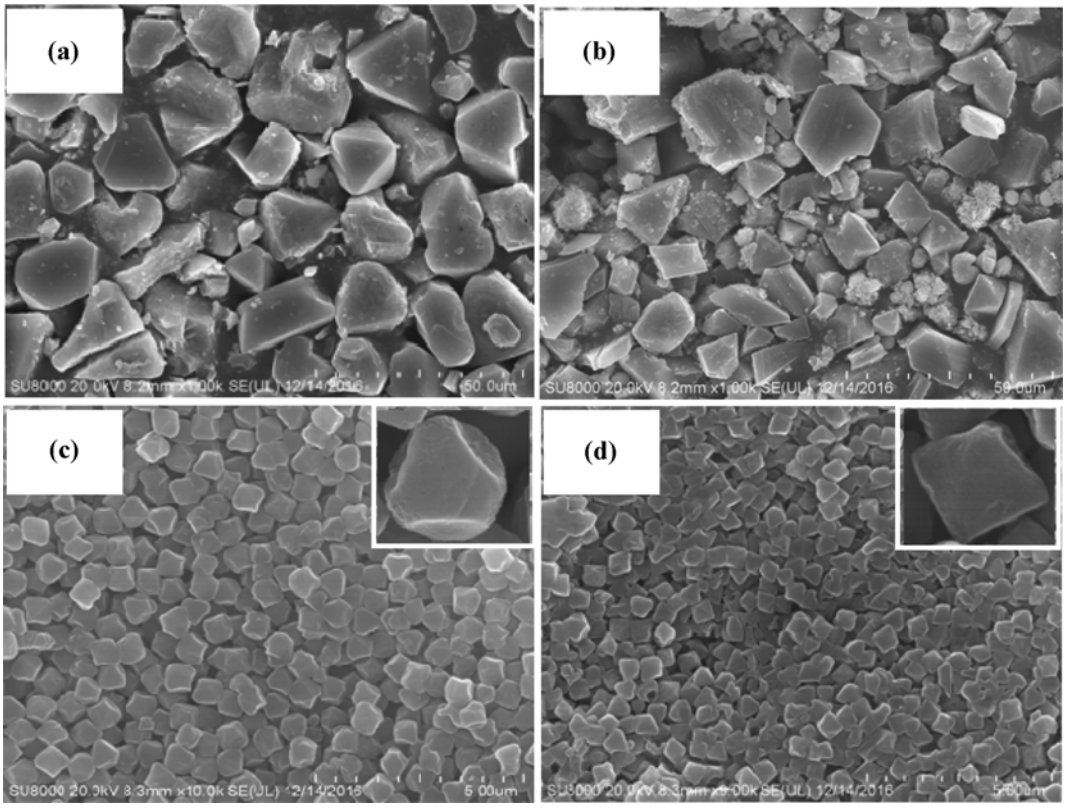

Fig. 1. The SEM images of Cu-BTC particles under different synthesis conditions: (a) Sample A (120 °C-72 hrs-no PVP); (b) sample B (120 °C-4 hrs-no PVP); (c) sample B (120 °C-4 hrs-PVP); (d) sample B (100 °C-4 hrs-PVP).

Cu-BTC nanoparticles. Meanwhile, the utilization of PVP can also decrease the particle size of Cu-BTC remarkably. Here a lower synthesis temperature was adopted to prepare sample D in our experiment. As shown in Fig. 1(d), the particle size of sample D is approximately 530 nm, which is slightly smaller than that of sample C. In addition, well-defined octahedral morphologies could be obtained for sample D. In our experiment, the synthesis conditions of sample D were adopted. XRD patterns of sample D are given in Fig. 2. Fig. 2 shows that both samples A and D exhibit the typical topological structure of Cu-BTC [32-35].

2. Effect of Annealing Temperature on Cu-based Composite Nanoparticles

Herein the effect of annealing temperature on phase structure of Cu-based composite nanoparticles was investigated under pure nitro-

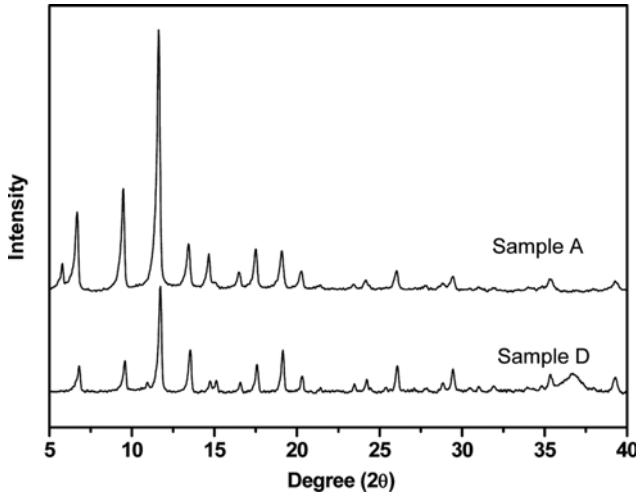

Fig. 2. The XRD patterns of A-Cu-BTC sample and D-Cu-BTC sample from different synthesis conditions: (A) Sample A (120 °C-72 hrs-no PVP); (D) Sample D (100 °C-4 hrs-PVP).

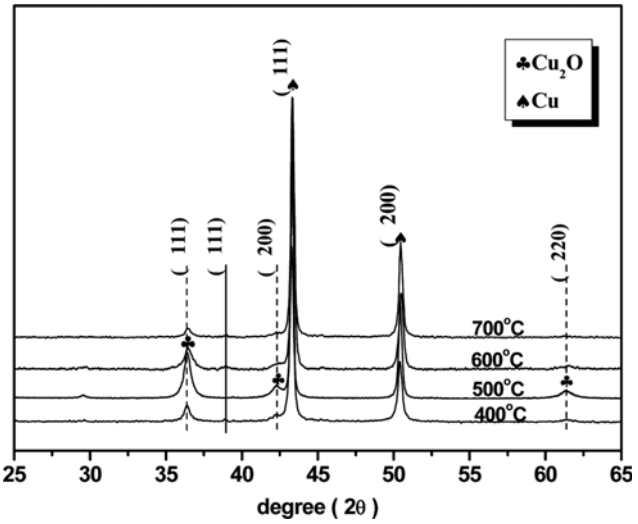

Fig. 3. XRD patterns of different samples at different annealing temperature.

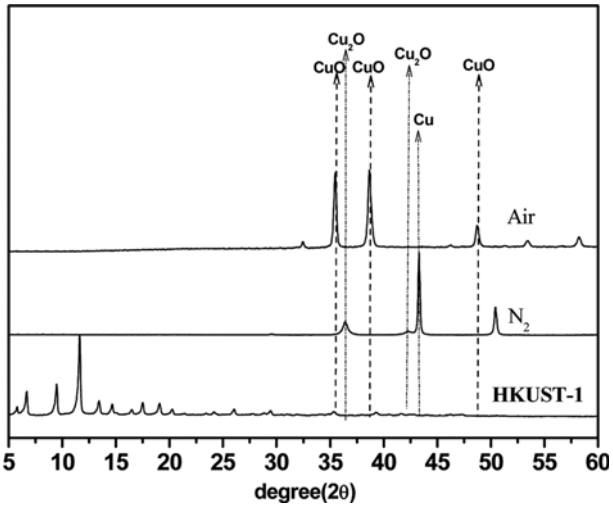

Fig. 4. XRD patterns of two samples prepared under air and nitrogen annealing atmospheres.

gen atmosphere. The XRD patterns of Cu-based composite nanoparticles at 400 °C, 500 °C, 600 °C and 700 °C are shown in Fig. 3. Two sharp diffraction peaks at 43° and 50° can be ascribed to the crystal planes of (111) and (200) of Cu (JCPDS card no. 04-0836), respectively. With annealing temperature increasing from 400 °C to 700 °C, the diffraction intensity of Cu phase gradually increases. The XRD patterns of Cu_2O also can be observed at 400 °C, 500 °C, 600 °C and 700 °C, in which the diffraction peaks at 36.37°, 42.22° and 61.30° can be ascribed to the crystal planes of (111), (200) and (220) of Cu_2O (JCPDS card no. 04-0836), respectively. It means that Cu^{2+} in Cu-BTCs can be effectively reduced during pyrolyzing Cu-BTC ligands. Note that the most remarkable diffraction peaks of Cu_2O phase were obtained at 500 °C. However, Cu still accounts for the majority of composite nanoparticles during the whole process. Nearly no diffraction peaks of CuO can be detected from 400 °C to 700 °C [36]. The experimental results show that the annealing temperature cannot effectively optimize the composition of Cu-based nanoparticles.

In our experiment, Cu-BTC was further pyrolyzed under air and pure nitrogen at 500 °C, respectively. The XRD patterns of two samples are given in Fig. 4. It can be found that Cu-BTC was transformed into CuO phase under air and Cu/Cu_2O binary phase under

Table 3. Annealing gas composition of different samples

Sample	Precursor	Temperature (°C)	Gas atmosphere ($ml \cdot min^{-1}$)
S-40	Cu-BTC	500	40(N_2): 2(air)
S-80	Cu-BTC	500	80(N_2): 2(air)
S-120	Cu-BTC	500	120(N_2): 2(air)
S-160	Cu-BTC	500	160(N_2): 2(air)
S-200	Cu-BTC	500	200(N_2): 2(air)

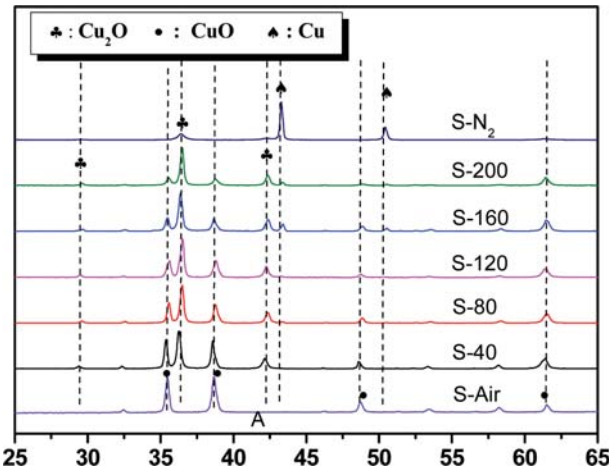

Fig. 6. XRD patterns of different samples fabricated under different mixed annealing atmosphere of nitrogen and air: S-N_2 sintered under pure nitrogen; S-200 sintered under a mixed gas of 200 $ml \cdot min^{-1}$ nitrogen and 2 $ml \cdot min^{-1}$ air; S-160 sintered under a mixed gas of 160 $ml \cdot min^{-1}$ nitrogen and 2 $ml \cdot min^{-1}$ air; S-120 sintered under a mixed gas of 120 $ml \cdot min^{-1}$ nitrogen and 2 $ml \cdot min^{-1}$ air; S-80 sintered under a mixed gas of 80 $ml \cdot min^{-1}$ nitrogen and 2 $ml \cdot min^{-1}$ air; S-40 sintered under a mixed gas of 40 $ml \cdot min^{-1}$ nitrogen and 2 $ml \cdot min^{-1}$ air; S-air sintered under air.

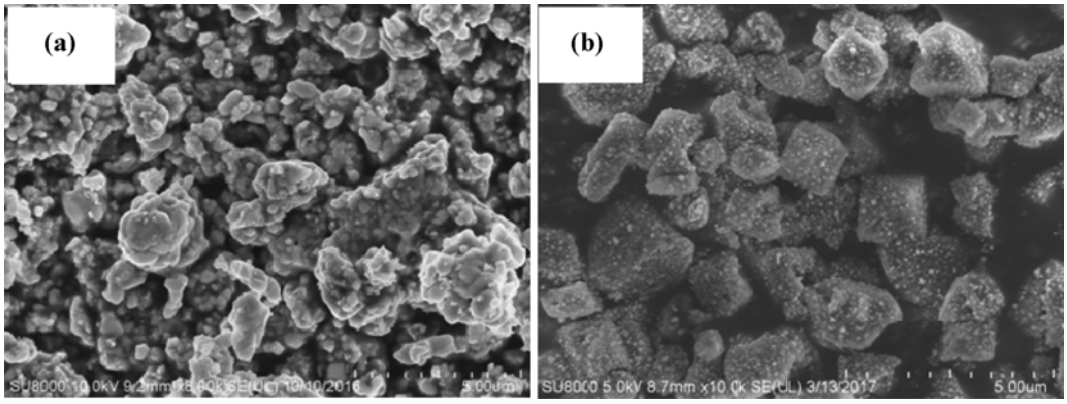

Fig. 5. SEM images of two samples prepared under air and nitrogen atmospheres: (a) The sample sintered under air; (b) the sample sintered under nitrogen.

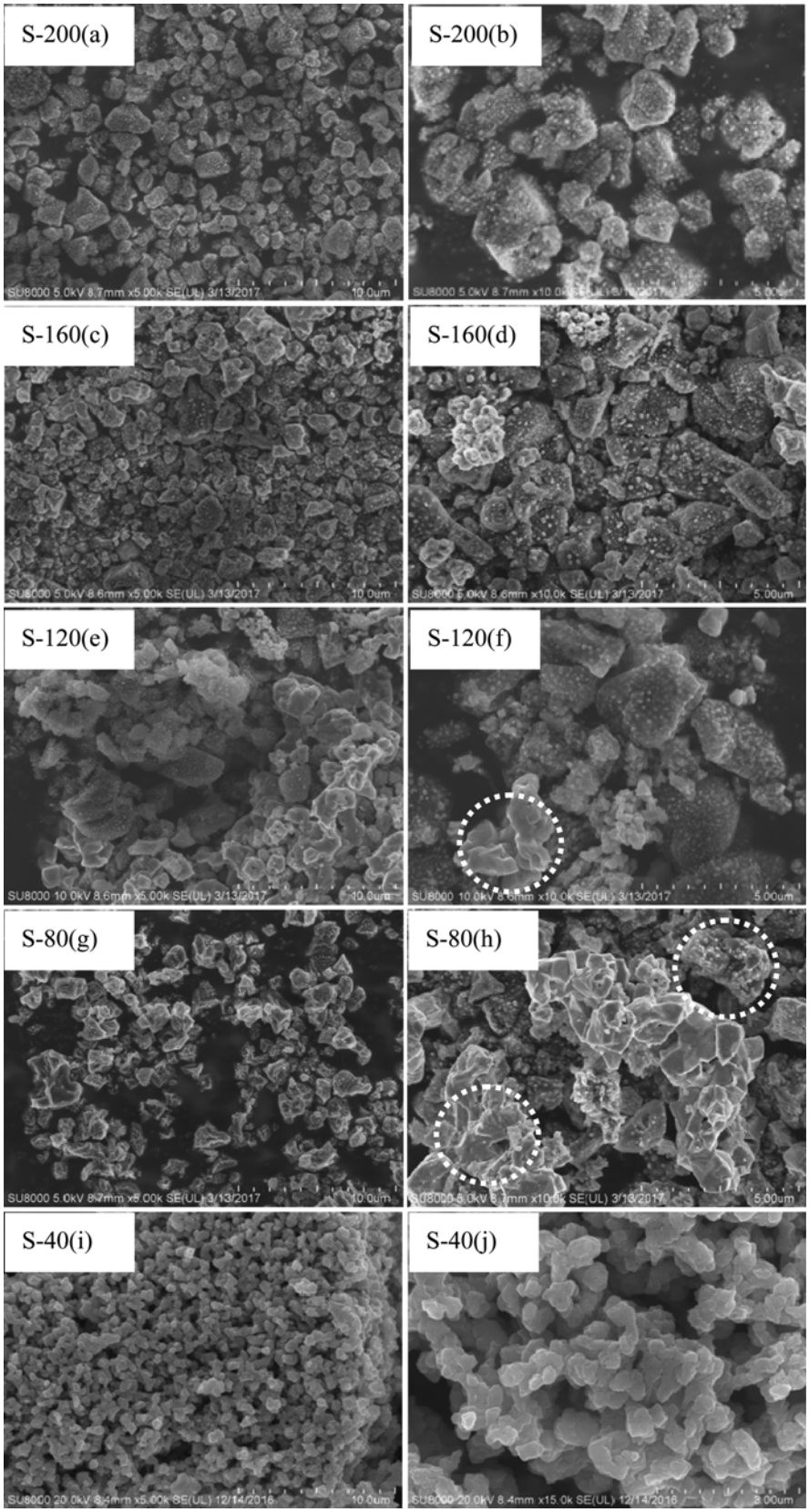

Fig. 7. SEM images of different samples fabricated under different mixed annealing atmosphere of nitrogen and air: (a), (b) S-200 sintered under a mixed gas of 200 ml·min^{-1} nitrogen and 2 ml·min^{-1} air; (c), (d) S-160 sintered under a mixed gas of 160 ml·min^{-1} nitrogen and 2 ml·min^{-1} air; (e), (f) S-120 sintered under a mixed gas of 120 ml·min^{-1} nitrogen and 2 ml·min^{-1} air; (g), (h) S-80 sintered under a mixed gas of 80 ml·min^{-1} nitrogen and 2 ml·min^{-1} air; (i), (j) S-40 sintered under a mixed gas of 40 ml·min^{-1} nitrogen and 2 ml·min^{-1} air.

N_2. The SEM images of two samples are presented in Fig. 5. As shown in Fig. 5(a), CuO phase obtained from air pyrolysis exhibits flower-like morphology. EDS analysis from Fig. S1(a) and Table 2 shows that the copper content in CuO is about 75.82 At%, whereas the carbon content is only 8.12 At%. The EDS elemental analysis shows that the most carbons in Cu-BTC can be oxidized into CO_2 under air. Fig. 5(b) depicts the surface morphology of Cu-based nanoparticles from N_2 pyrolysis. It can be found that the obtained Cu-based nanoparticles maintain the original polyhedral shape of Cu-BTC. Meanwhile, a large amount of nanoparticles are anchored into polyhedral carbon skeletons. The EDS elemental analysis in Fig. S1(b) and Table 2 proved that the carbon skeletons can be well preserved under nitrogen atmosphere, where the carbon content accounts for 73.33 At% and copper content is only about 9.08 At%. One problem is that Cu phase accounts for the majority of Cu-based composite nanoparticles under nitrogen atmosphere, and it is difficult to adjust the composition of $Cu/Cu_2O/CuO$ ternary nanoparticles.

3. Effect of Annealing Atmosphere on Cu-based Composite Nanoparticles

Although Cu-based composite nanoparticles can be obtained under pure N_2 atmosphere, Cu accounts for the majority in composite nanoparticles. Hence, it is necessary to improve CuO or Cu_2O content and produce more $Cu/Cu_2O/CuO$ hetero-junctions. Herein, trace amounts of air were added into nitrogen annealing atmosphere. As shown in Table 3, several samples were obtained by changing the annealing gas composition.

The XRD patterns of all the samples obtained at different annealing atmosphere are shown in Fig. 6. It can be observed that the addition of air into pure nitrogen can obviously influence the phase structure of Cu-composite nanoparticles. The S-N_2 only exhibit Cu phase and little Cu_2O phase. S-200 samples were obtained under a mixed atmosphere of 200 ml·min^{-1} N_2 and 2 ml·min^{-1} air. As shown in Fig. 6, the diffraction peak intensity of Cu phase obviously decreases and the diffraction peak intensity of Cu_2O gradually increases. Meanwhile, the typical diffraction peaks of CuO phase are also present in S-200. The experimental results proved that the addition of trace air can remarkably change the composition of Cu-based nanoparticles. S-160 sample was fabricated under a mixed annealing gas of 160 ml·min^{-1} N_2 and 2.0 ml·min^{-1} air. As shown in Fig. 6, the respective typical peaks of Cu, Cu_2O and CuO phase can be clearly identified. While more air was added into the annealing atmosphere, S-120 was obtained. As expected, the diffraction peaks of Cu phase obviously decrease and CuO phase increases, indicating that a small quantity of air in annealing gas can induce more Cu phase transformed into CuO phase. Interestingly, Cu_2O phase in S-120 accounts for the majority of $Cu/Cu_2O/CuO$ composite nanoparticles. S-80 and S-40 samples were obtained by further increas-

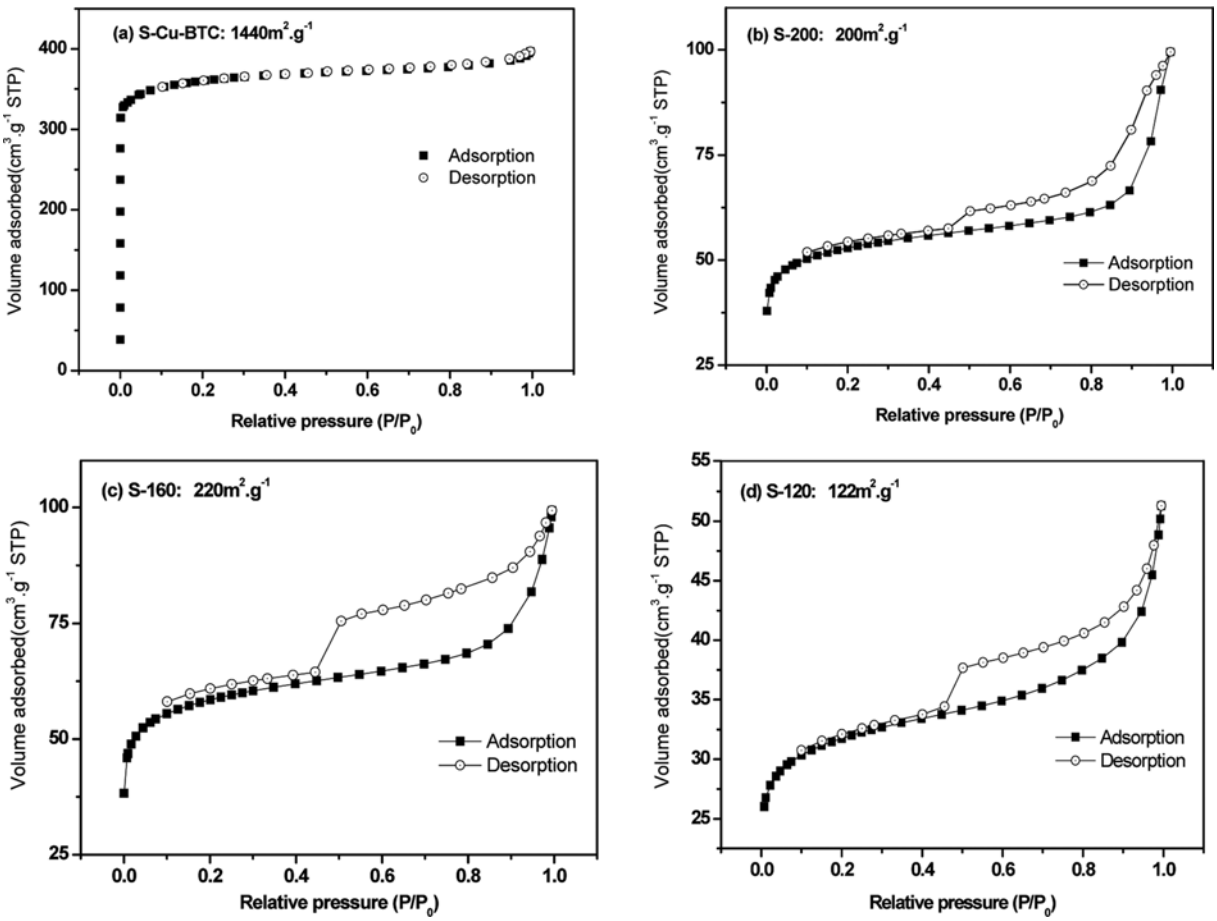

Fig. 8. Nitrogen adsorption isotherms at 77 K for S-BTC, S-200, S-160 and S-120.

ing air in the annealing gas. As shown in Fig. 6, the peak intensity of CuO continuously increases, and finally no Cu phase can be detected for S-80 and S-40. Both S-80 and S-40 exhibit a mixed phase of Cu_2O and CuO, whereas Cu_2O still maintains a majority in Cu_2O/CuO binary nanoparticles. While Cu-BTC was annealed under air, S-air sample could be obtained which displays a single CuO phase. The experimental result shows that the composition of Cu-based composite nanoparticles can be rationally modulated by changing the proportion of nitrogen and air in annealing stream.

SEM images of different samples obtained by changing annealing stream are shown in Fig. 7. S-200 and S-160 still maintain the original polyhedral shapes like Cu-BTC, which indicates that the porous carbon skeletons still can be well preserved under a mixed annealing stream at 500 °C. As shown in Fig. 7(a)-(d), a number of Cu, Cu_2O or CuO nanoparticles are highly distributed into S-200 and S-160 samples. While more air was added into the annealing atmosphere, S-120, S-80 and S-40 samples could be obtained. In Fig. 7(e) and (f), S-120 exhibits irregular porous carbon morphology. Especially, S-80 sample is composed of two different crystallites: one crystallite can be ascribed to porous carbon supported Cu-based nanoparticles, and the other one belongs to inorganic CuO/Cu_2O composites (Fig. 7(g), (h)). S-40 was obtained under 40 $ml \cdot min^{-1}$ N_2 and 2 $ml \cdot min^{-1}$ air. In Fig. 7(i), (j) the addition of more air in the annealing gas completely changes the surface morphology of Cu-based composite nanoparticles, which indicates that the organic groups of Cu-BTC can be nearly oxidized into CO_2 under a mixed annealing atmosphere composed of 40 $ml \cdot min^{-1}$ N_2 and 2 $ml \cdot min^{-1}$ air.

N_2 adsorption isotherms at 77 K for Cu-BTC, S-200, S-160 and S-120 are depicted in Fig. 8. As shown in Fig. 8(a), the BET specific surface area of Cu-BTC was calculated to be 1,440 $m^2 \cdot g^{-1}$, which is consistent with other published papers. Fig. 8(b) shows that the BET specific surface area of S-200 was about 200 $m^2 \cdot g^{-1}$. The BET measurement indicates that porous carbon support with high specific surface area can be well preserved although Cu-BTCs were pyrolyzed at a mixed atmosphere. Interestingly, S-160 exhibits a higher BET specific surface area of 220 $m^2 \cdot g^{-1}$ (seen in Fig. 8(c)). In addition, obvious hysteresis loops in BET isotherms can be found for S-200 and S-160, which indicates that the addition of a small quantity of oxygen in nitrogen annealing atmosphere can generate more mesopores in porous carbon skeletons. However, with more air addition in the mixed annealing stream such as S-120, its BET specific surface area dramatically drops to be about 122 $m^2 \cdot g^{-1}$. This experimental result illustrates that the addition of excessive air can degrade the pore structure of the porous carbon support, which is consistent with the upward SEM characterization.

S-160 sample was selected to perform HR-TEM characterization. Fig. 9 presents the interior microstructure and particle distribution of S-160. As shown in Fig. 9(a), a thin carbon layer covers the underlying Cu-based nanoparticles (Cu, Cu_2O and CuO). The magnified surface morphology can be clearly observed in Fig. 9(b). The porous carbon support exhibits stripe-shaped morphology, and a large number of nanoparticles are uniformly anchored into porous carbon support. The interior microstructure of porous carbon supports can be distinctly observed in Fig. 9(c). It can be found that the particle size of $Cu/Cu_2O/CuO$ ternary nanoparticles is about 10-30 nm, which is consistent with the calculated average particle size of XRD (25.6 nm). Meanwhile, these $Cu/Cu_2O/CuO$

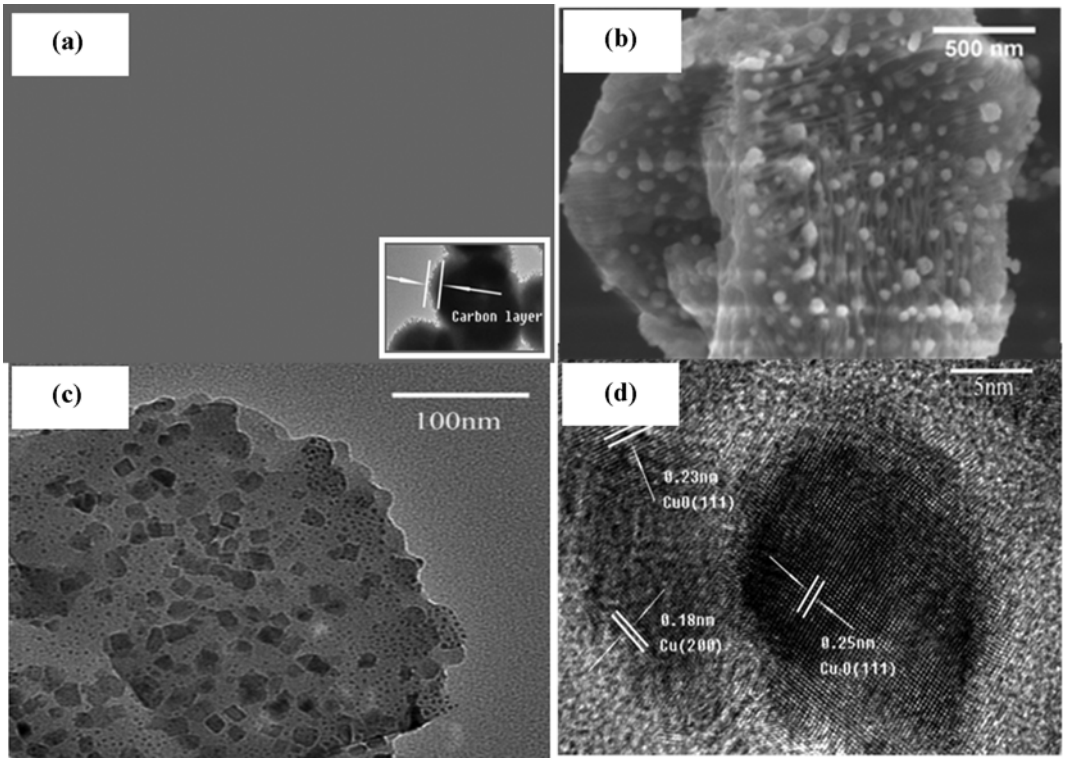

Fig. 9. HR-TEM images of S-160 sample: S-160 sintered under a mixed gas of 160 $ml \cdot min^{-1}$ nitrogen and 2 $ml \cdot min^{-1}$ air.

composite nanoparticles are uniformly dispersed in the interior of porous carbon without any agglomeration. Fig. 9(d) shows the presence of many obvious hetero-junctions of Cu/Cu_2O/CuO ternary nanoparticles, where the interlaced boundaries marked by dash lines mean the formation of Cu/Cu_2O/Cu composite nanoparticles.

S-160 sample was chosen to conduct SEM-EDS elemental analysis. In Fig. S2(a), (b) the porous carbon is composed of three kinds of elements: copper, oxygen and carbon. The distribution of three elements in porous carbon can be clearly observed from Fig. S2(c)-(f), where cooper, oxygen and copper are mixed homogeneously together. EDS elemental analysis further indicates that Cu, Cu_2O and Cu nanoparticles are highly dispersed in porous carbon without any agglomeration.

4. Catalytic Test of Cu/Cu_2O/CuO Ternary Nanoparticles

Catalytic reduction of nitroarenes into the corresponding amines was considered as a green route by precious metallic nanoparticles. However, the high cost of precious metals compels researchers to develop some alternative cost-effective catalysts [37-39]. We investigated the catalytic activity of porous carbon supported Cu/Cu_2O/CuO ternary nanoparticles.

The reduction of *p*-nitrophenol was conducted using $NaBH_4$ as reducing agent in aqueous medium. The reaction can be monitored in real time by measuring the absorption peak intensity at 400 nm in UV-*visible* spectrum. Note that the strongest absorption peak of *p*-nitrophenol is supposed to be at 317 nm, but it will red-shift to about 400 nm with the addition of $NaBH_4$ owing to the formation of 4-nitrophenolate [40]. While copper-base nanoparticles are introduced into the reaction solution, the yellow color of the mixture gradually become fading and the absorption peak intensity at 400 nm deceases, which implies the reduction of *p*-nitrophenol concentration. Meanwhile, the intensity of another absorption peak at 300 nm can increase, indicating the formation of *p*-aminophenol.

Fig. S3 and Fig. 10 show the representative UV-*visible* spectra for the reduction of *p*-nitrophenol. All samples exhibit certain catalytic activity in catalytic reduction of *p*-nitrophenol, but their catalytic activities are much different. The catalytic activity order was S-160>S-200>S-N_2>S-120>S-80>S-40. As shown in Fig. 6, S-80 and S-40 contain only CuO and Cu_2O phase. Hence, both S-80 and S-40 display lower catalytic ability. Furthermore, S-40 exhibits lower activity compared with S-80. This experimental result shows that the optimized phase composition for copper-base nanoparticles can endow a higher catalytic activity in the reduction of *p*-nitrophenol due to better accessibility of Cu/Cu_2O/CuO hetero-junctions. S-160, S-200, S-N_2 and S-120 exhibit similar polyhedral porous carbon shapes, but S-160 exhibits the highest catalytic activity, which can be ascribed to the better synergistic effect of Cu/Cu_2O/CuO ternary nanoparticles. For example, although S-N_2 preserves excellent porous polyhedral carbon shape, Cu accounts for the majority of the Cu-based composite nanoparticles and only a little Cu_2O can be found in S-N_2. The experimental results show that the optimized synergistic effect of Cu-based composite nanoparticles plays an important role in the catalytic reduction of *p*-nitrophenol. Fig. S4 shows a comparative result between S-160 and CuO(S-air). It takes only 3 min for S-160 to completely reduce *p*-nitrophenol, but CuO(S-air) catalyst reduces the half of *p*-nitrophenol for more than 3.5 min. A comparative experiment indicates that the catalytic activity of S-160 is much higher than CuO(S-air), indicating that the synergistic effect of Cu, Cu_2O and CuO in S-160 plays an important role in the catalytic reduction of p-nitrophenol. A proposed mechanistic reason is that copper in Cu/Cu_2O/CuO ternary nanoparticles is a good electrical conductor which easily transfers electrons from one adsorbed species on its surface to another. The Cu/Cu_2O/CuO hetero-junctions in S-160 can supply more Cu active sites from Cu_2O/CuO during catalytic reduction. Moreover, the oxidation of Cu species can be effectively inhibited via the synergistic effect of Cu/Cu_2O/CuO ternary nanoparticles. Hence, S-160 catalyst exhibits higher catalytic activity in p-nitrophenol reduction.

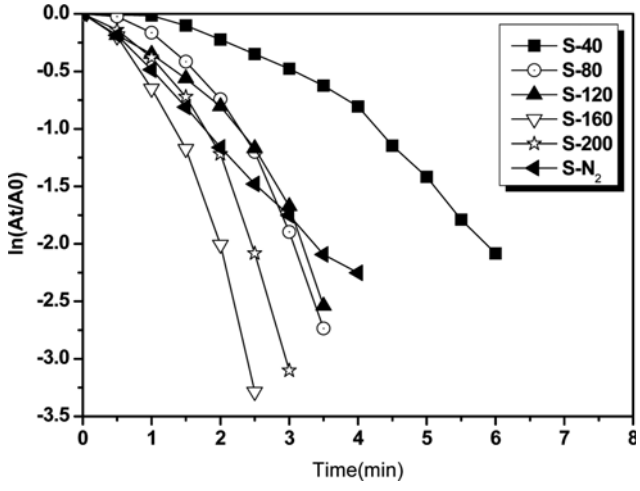

Fig. 10. Plots of $\ln(A_t/A_0)$ versus time for the catalytic reduction of *p*-nitrophenol at room temperature with different catalysts.

CONCLUSION

Well-defined Cu-BTC particles were first synthesized via solvothermal method. Then carbon-supported Cu/Cu_2O/CuO ternary nanoparticles were successfully prepared by annealing Cu-based MOFs. It was found that the addition of PVP in precursor solution can obtain smaller and more uniform Cu-BTC particles. Based on these optimized Cu-BTC particles, we rationally realized the composition optimization of CuO/Cu_2O/Cu ternary nanoparticles supported onto porous carbon by simply modulating the composition of annealing stream. XRD and SEM measurement shows that adjusting the annealing stream is a more effective approach to modulating Cu/Cu_2O/CuO ternary nanoparticles compared with annealing temperature. The addition of trace air in annealing stream can improve Cu_2O phase and decrease Cu phase. In an optimized mixed annealing stream, porous carbon support can be well preserved and even exhibit higher specific surface area (220.07 $m^2 \cdot g^{-1}$). However, the addition of excessive air can produce only Cu_2O/CuO diphasic particles or even CuO single phase. Accordingly, porous carbon skeletons gradually degrade. For an optimized sample such as S-160, its average particle size is only 25.6 nm, which is highly dispersed into the carbon support. Meanwhile, the hetero-junction boundaries of Cu/Cu_2O/CuO in S-160 can be clearly observed. In the catalytic experiment, the order of catalytic activity of porous

carbon-supported copper-based nanoparticles is highly relevant to the synergistic effect of Cu, Cu_2O and CuO. Porous carbon-supported Cu/Cu_2O/CuO ternary nanoparticles exhibit higher activity than Cu_2O/CuO diphasic or CuO single particles. Especially, it takes only 3.5 min for S-160 to completely reduce the *p*-nitrophenol. In summary, this article provides a new strategy for rationally modulating the composition of Cu/Cu_2O/CuO nanoparticles encapsulated in the porous carbon support skeleton.

ACKNOWLEDGEMENTS

This work was supported by National Natural Science Foundation (21703091, 21201096) and the education department of Liaoning Province, China (LZ2015050). The authors are also grateful for the financial support from the National Natural Science Foundation of China (No. 21103077), program for New Century Excellent Talents in University (No. NCET-11-1011), and the support from Key Laboratory of Coal to Ethylene Glycol and Its Related Technology, Chinese Academy of Sciences.

SUPPORTING INFORMATION

Additional information as noted in the text. This information is available via the Internet at http://www.springer.com/chemistry/journal/11814.

REFERENCES

1. J. Hu, N. Jiang, J. Li, K. Shang, N. Lu and Y. Wu, *J. Chem. Eng. J.*, **293**, 216 (2016).
2. K. Piwowar, A. Blacha-Grzechnik, P. Bernas and J. Zak, *Appl. Surf. Sci.*, **359**, 426 (2015).
3. D. Juretic, H. Kusic, D. D. Dionysiou, B. Rasule and A. Loncaric Bozic, *J. Chem. Eng.*, **257**, 229 (2014).
4. J. H. Noh and R. Meijboom, *Appl. Surf. Sci.*, **320**, 400 (2014).
5. V. K. Gupta, N. Atar, M. L. Yola, Z. Üstündağ and L. Uzun, *Water Res.*, **48**, 210 (2014).
6. U. Kurtan and A. Baykal, *Mater. Res. Bull.*, **60**, 79 (2014).
7. Z. Hasan, D. W. Cho, C. M. Chon, K. Yoon and H. Song, *J. Chem. Eng.*, **298**, 183 (2016).
8. B. Nabil, M. N. Morshed, E. A. Ahmida, B. Nemeshwaree, C. Christine, V. Julien, T. Olivier and A. Abdelkrim, *Chem. Eng. J.*, **356**, 702 (2019).
9. M. A. Bhosale, S. S. R. Gupta and B. M. Bhanage, *Polyhedron*, **120**, 96 (2016).
10. B. Nabil, E. A. Ahmid, C. Christine, V. Julien and A. Abdelkrim, *Chem. Eng. J.*, **351**, 328 (2018).
11. R. J. Kongarapu, P. Mahamallik and A. Pal, *J. Environ. Chem. Eng.*, **5**, 1321 (2017).
12. J. G. You, C. Shanmugam, Y. W. Liu, C. J. Yu and W. L. Tseng, *J. Hazard. Mater.*, **324**, 420 (2017).
13. R. Krishna, D. M. Fernandes, J. Ventura, C. Freire and E. Titus, *Int. J. Hydrogen Energ.*, **41**, 11608 (2016).
14. T. Aditya, A. Pal and T. Pal, *Chem. Commun.*, **51**, 9410 (2015).
15. M. Moeinian and K. Akhbari, *J. Solid State Chem.*, **225**, 459 (2015).
16. N. Bouazizi, J. Vieillard, P. Thebault, F. Desriac, T. Clamens, R. Bargougui, N. Couvrat, O. Thoumire, N. Brun, G. Ladam, S. Morin, N. Mofaddel, O. Lesouhaitier, A. Azzouz and F. Le Derf, *Dalton T.*, **47**, 9143 (2018).
17. M. Tang, S. Zhang, X. Li, X. Pang and H. Qiu, *Mater. Chem. Phys.*, **148**, 639 (2014).
18. L. Yuan, Q. Yin, Y. Wang and G. Zhou, *Chem. Phys. Lett.*, **590**, 92 (2013).
19. A. Ajmal, I. Majeed, R. N. Malik, M. Iqbal, M. A. Nadeem, I. Hussain, S. Yousaf, Zeshan, G. Mustafa, M. I. Zafar and M. A. Nadeem, *J. Enviorn. Chem. Eng.*, **4**, 2138 (2016).
20. M. E. El-Naggar, A. G. Hassabo, A. L. Mohamed and T. I. Shaheen, *J. Colloid Interf. Sci.*, **498**, 413 (2017).
21. G. M. Alvarenga, I. B. Coutinho Gallo and H. M. Villullas, *J. Catal.*, **348**, 1 (2017).
22. L. Rout, A. Kumar, R. S. Dhaka, G. N. Reddy, S. Giri and P. Dash, *Appl. Catal. A-Gen.*, **538**, 107 (2017).
23. R. Hosseinpour, A. Pineda, A. Garcia, A. A. Romero and R. Luque, *Catal. Commun.*, **48**, 73 (2014).
24. Y. Wang, G. Li, J. Jin and S. Yang, *Int. J. Hydrogen Energy*, **42**, 5938 (2017).
25. X. Wei, H. Li, C. e. Yuan, Q. Li and S. Chen, *Micropor. Mesopor. Mater.*, **118**, 307 (2009).
26. Y. Liu, J. Liu and Y. S. Lin, *Micropor. Mesopor. Mater.*, **214**, 242 (2015).
27. J.-B. Raoof, S. R. Hosseini, R. Ojani and S. Mandegarzad, *Energy*, **90**, Part 1 1075 (2015).
28. C. Chmelik, *Micropor. Mesopor. Mater.*, **216**, 138 (2015).
29. Y. Liu, J. Xu and S. Liu, *Micropor. Mesopor. Mater.*, **236**, 94 (2016).
30. W. Bak, H. S. Kim, H. Chun and W. C. Yoo, *Chem. Commun.*, **51**, 7238 (2015).
31. R. Zhang, L. Hu, S. Bao, R. Li, L. Gao, R. Li and Q. Chen, *J. Mater. Chem. A*, **4**, 8412 (2016).
32. J. B. DeCoste, J. M. S. Denny, G. W. Peterson, J. J. Mahle and S. M. Cohen, *Chem. Sci.*, **7**, 2711 (2016).
33. S. El-Hankari, J. Huo, A. Ahmed, H. Zhang and D. Bradshaw, *J. Mater. Chem. A*, **2**, 13479 (2014).
34. S. Liu, L. Sun, F. Xu, J. Zhang, C. Jiao, F. Li, Z. Li, S. Wang, Z. Wang, X. Jiang, H. Zhou, L. Yang and C. Schick, *Energy Environ. Sci.*, **6**, 818 (2013).
35. D. Bradshaw, A. Garai and J. Huo, *Chem. Soc. Rev.*, **41**, 2344 (2012).
36. Y. Wang, Y. Lu, W. Zhan, Z. Xie, Q. Kuang and L. Zheng, *J. Mater. Chem. A*, **3**, 12796 (2015).
37. A. K. Sasmal, S. Dutta and T. Pal, *Dalton. T.*, **45**, 3139 (2016).
38. X. Shi, F. Zheng, N. Yan and Q. Chen, *Dalton. T.*, **43**, 13865 (2014).
39. M. Liu, L. Lv, X. Du, J. Lang, Y. Su, Y. Zhao and X. Wang, *Rsc. Adv.*, **5**, 103013 (2015).
40. K. Layek, M. L. Kantam, M. Shirai, D. Nishio-Hamane, T. Sasaki and H. Maheswaran, *Green Chem.*, **14**, 3164 (2012).

Supporting Information

Composition modulation of $Cu/Cu_2O/CuO$ nanoparticles supported on carbon for *p*-nitrophenol reduction

Jia Li, Wei Liu, Yongxin Ding, Likui Liu, Fang Li, and Qiming Li†

College of Chemistry, Chemical Engineering and Environmental Engineering, Liaoning Shihua University, Fushun Liaoning 113001, P. R. China

(*Received 21 January 2019 • accepted 9 April 2019*)

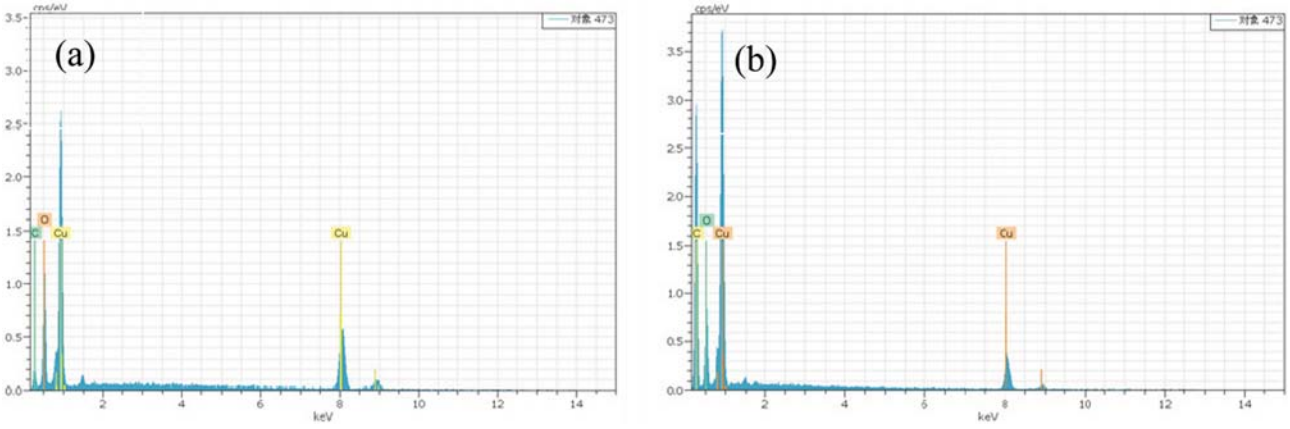

Fig. S1. SEM-EDS elemental analysis of two samples prepared under air and nitrogen atmospheres: (a) The sample sintered under air; (b) the sample sintered under nitrogen.

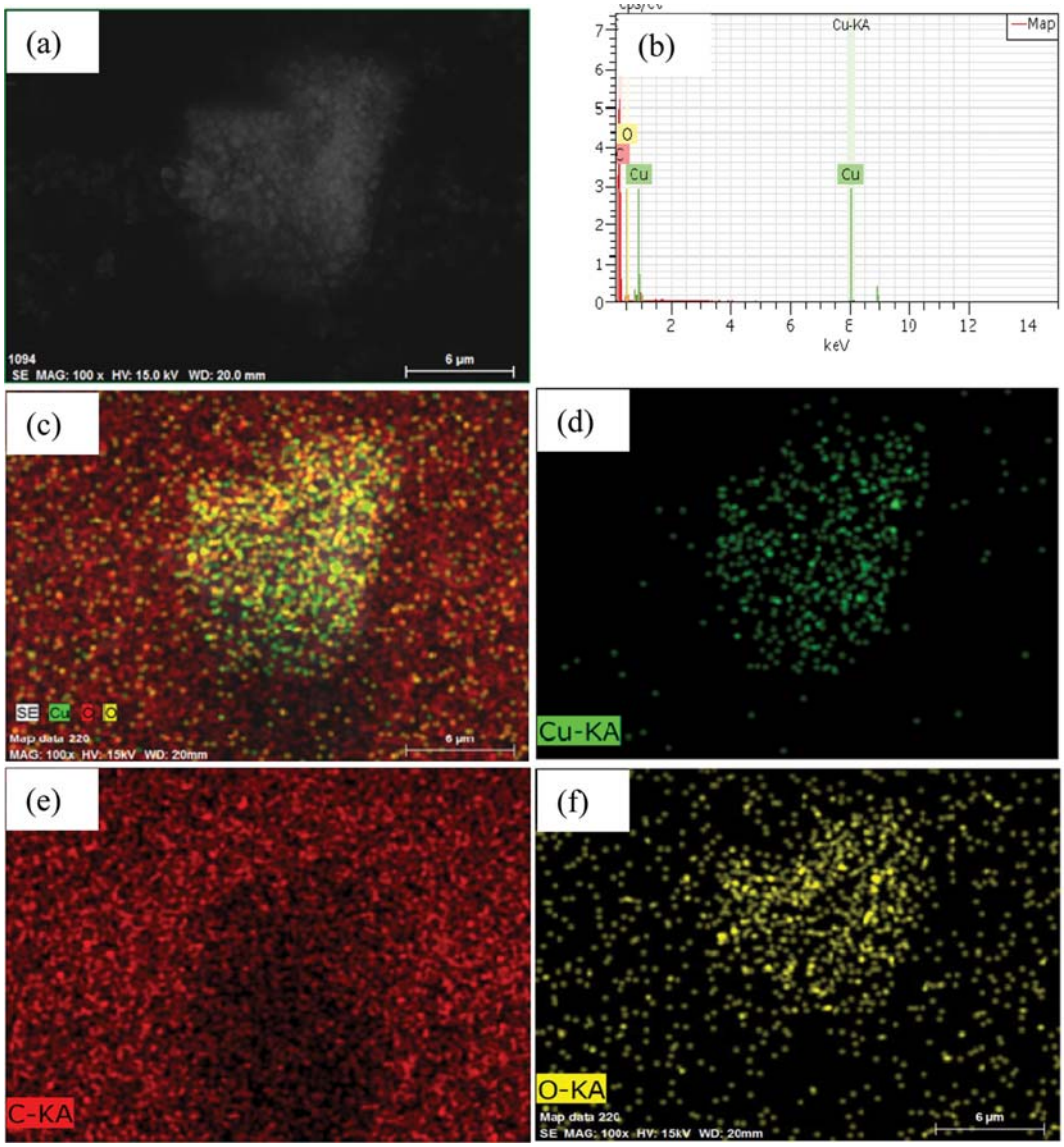

Fig. S2. SEM-EDS images of S-160 sample: (a) SEM image of S-160; (b) EDS elemental analysis of S-160; (c) EDS elemental distribution of S-160; (d) copper elemental distribution in S-160; (e) carbon elemental distribution in S-160; (f) oxygen elemental distribution in S-160.

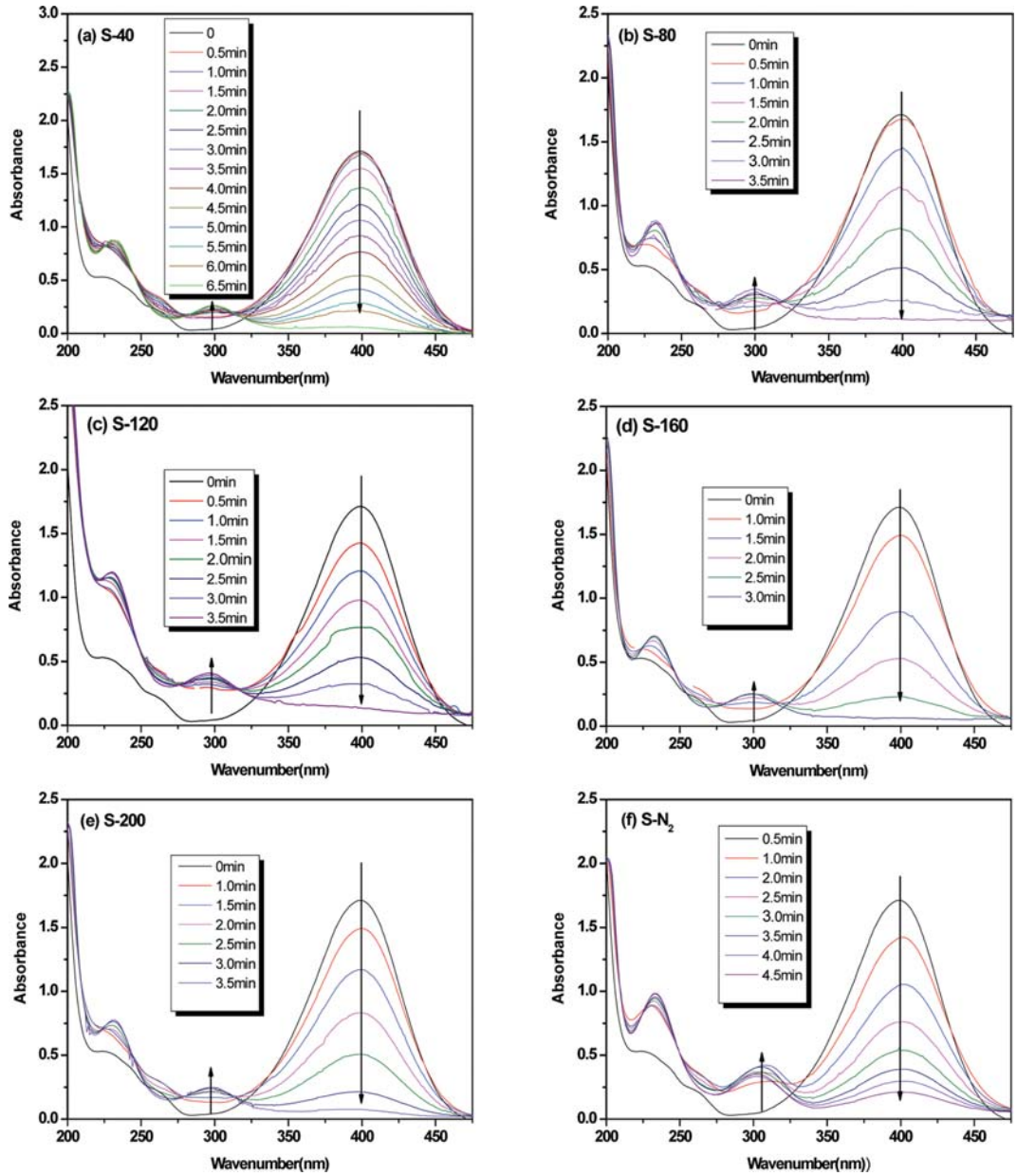

Fig. S3. UV-visible absorption spectra of the catalytic reduction of *p*-nitrophenol by $NaBH_4$ using different catalysts.

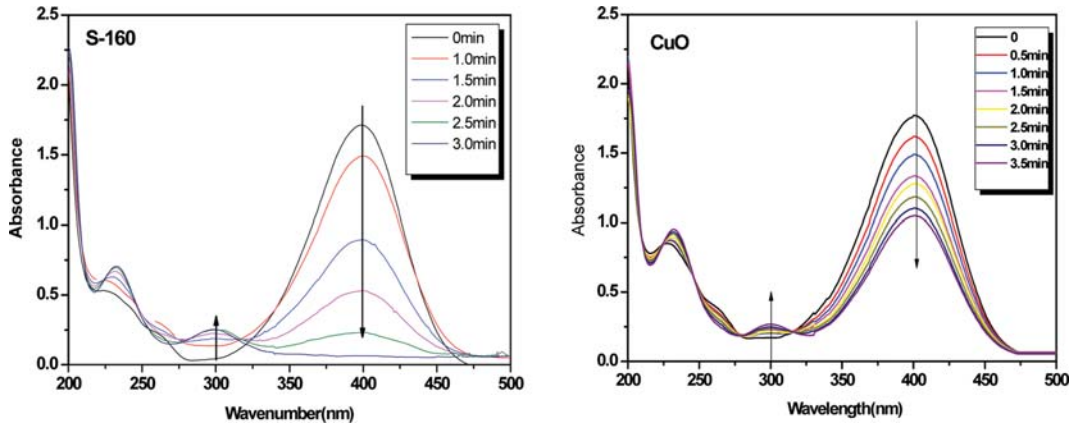

Fig. S4. Comparative result of catalytic reduction of *p*-nitrophenol using S-160 and CuO catalysts.